Particle simulation of two dimensional dust crystal formation in a mesothermal plasma flow

F. Melandsø[a)]
The Auroral Observatory, University of Tromsø, N-9037 Tromsø, Norway

J. Goree[b)]
Department of Physics and Astronomy, The University of Iowa, Iowa City, Iowa 52242

(Received 4 October 1995; accepted 13 December 1995)

A two-dimensional simulation is used to study the crystallization of strongly coupled dusty plasmas. The dust grains are simulated as particles, while the electrons and ion solutions are obtained from fluid equations. We model gas discharges with dust particles confined in the sheath and at the sheath edge. In these regions the ions flow past the dust grains at a velocity v_0 that typically is mesothermal, $v_{Ti} \ll v_0 \ll v_{Te}$. A negative charged dust particle will under these conditions focus the ions, creating a local maximum in the plasma potential on the downstream side of the particle. This maximum means that there is an anisotropic interparticle interaction, which can be manifested as an attractive interparticle force along the axis of the plasma flow. Our simulation shows that the equilibrium configuration of a dust crystal structure can be profoundly influenced by this asymmetry in the ion flow and plasma potential for certain charge to mass ratios for the dust particles. We initially distribute dust particles randomly in space with zero velocity and integrate their equations of motion, tracking their orbits as they settle into equilibrium positions. We show that there are several stable final equilibria, although they do not all have the same potential energy or probability of occurring. The most likely crystal configuration depends on the charge-to-mass ratio and the horizontal particle spacing of the grains. The vertically aligned columns of particles that have been observed in plasma crystal experiments are shown to be most likely for large dust charge-to-mass ratios.

I. INTRODUCTION

Dust particles in gas discharges are often confined in regions where the plasma has a mesothermal streaming velocity V_0 ($v_{Ti} \ll V_0 \ll v_{Te}$) towards the electrodes with respect to the thermal velocities of the ions v_{Ti} and electrons v_{Te}. Mesothermal flows around a solid object are characterized by an ion rarefaction in the wake followed by an ion focusing region, both of which contribute to a polarization of the plasma. This polarization is especially interesting since it causes the plasma potential to oscillate in position downstream of the particle. Oscillations or potential wells, as predicted both from a linear test particle approach[1] and from numerical calculations of nonlinear fluid equations,[2] may trap other dust particles if the thermal motion of dust is sufficiently low.

Laboratory experiments have revealed a significant anisotropy in the interparticle interactions in dusty plasmas.[3–9] These include vertically aligned particle in crystalline lattices and string-shaped coagulated particles. We have previously suggested[2] that the plasma anisotropy due to an ion flow may lead to these effects. In the case of the lattices, particles arrange in horizontal hexagons that often have an unexpected vertical alignment parallel to the flow rather than the staggered bcc or fcc structures that are expected if the interparticle potential is isotropic.[7–9]

Particle simulations have previously been used to study phase transitions and crystallization of dust particles.[10] The method suggested in Ref. 10, however, assumes symmetric shielding of the dust particles, which is unsuitable for drifting ion in the mesothermal regime.

For this article we have expanded the two-dimensional (2D) model used in Ref. 2 to include following the motion of the dust particles self-consistently from the forces acting on the particles. The numerical method is a quasiparticle simulation, where the plasma is represented by a fluid and the dust particles by N_p diffuse objects. In order to simulate levitation of dust outside an electrode surface, we have biased the potential on the outflowing boundary (simulating the electrode) negatively with respect to the potential on the inflowing side. Since this potential drop causes an electrostatic force acting on the dust particles opposite to the streaming direction, it may be balanced by the ion drag that occurs in our model. To make the simulation more realistic for larger dust particles, we have also included a gravitational force on the dust particles. Our simulations show that dust particles arrange themselves easily in a regular lattice, and that the potential wells predicted in Refs. 1 and 2 are, for some parameters, very important for dust particle alignment. Repeating several simulations with random initial spatial distributions of dust particles, we find a number of different 2D crystalline equilibria.

II. NUMERICAL MODEL

To model the dynamic of a strongly coupled dusty plasma, we have used a quasiparticle simulation where the

[a)]Electronic mail: frank@phys.uit.no
[b)]Electronic mail: goree@dusty.physics.uiowa.edu

plasma is described by a fluid while the dust particles are described by diffuse objects. This approach will include dust particle effects such as Coulomb collisions between dust grains, thereby allowing us to study the structure and dynamics of particles in crystallized and liquidlike dusty plasmas. Wave–particle interactions between the dust particles and the plasma fluid and the ion Coulomb drag are also incorporated to the extent possible while modeling ions as a fluid.

A. Plasma

The plasma is assumed to flow with a mesothermal velocity where the thermal effects from ions are assumed to be small. The ions can therefore be described by a cold fluid responding to the plasma potential ϕ according to the continuity and force equations

$$\partial_t n_i + \nabla(n_i \mathbf{v}_i) = 0, \tag{1}$$

$$\partial_t \mathbf{v}_i + \mathbf{v}_i \nabla \mathbf{v}_i = -\frac{eZ_i}{m_i} \nabla \phi. \tag{2}$$

Here n_i, $\mathbf{v}_i$, Z_i, and m_i are the ion density, velocity, electronic charge, and mass, respectively. We have assumed here that the dust particle radius a_d is much smaller than the electron Debye length λ_D and have neglected the ion loss into the dust particles. The ion loss into a dust particle causes an ion wake (rarefaction of the ion density) immediately downstream of the solid particle,[11,12] and this effect would obviously be lost in our model. However, for small dust particles ($a_d \ll \lambda_D$), the number of ions in this wake will contribute little to the asymmetrical potential around the dust particle.[2] The shape of the potential is mainly determined by ion focusing (included in our model) which appears regardless of the dust particle size.

The electrons are characterized simply by a prescribed uniform temperature T_e and a density given by the Boltzmann relation

$$n_e = n_0 \exp\left(\frac{e\phi}{KT_e}\right). \tag{3}$$

Here n_0 is the ion density at a point well away from any object in the plasma. The electron and ion densities are then included in the Poisson equation

$$\epsilon_0 \nabla^2 \phi = -e\left[n_i - n_e + Z_d \sum_{i=1}^{N_p} S_i(\mathbf{x})\right] \tag{4}$$

together with the space charge contribution from N_p dust particles with equal charge equal charges $Z_d e$. As in Ref. 2, we model the spatial distributions of the charge and ion absorption on a dust particle using a diffuse rather than discontinuous surface.

B. Dust particles

In our 2D simulation the diffuse objects are assumed to be infinite long cylinders aligned parallel to the electrode surface. Their surface charge and ion absorption is distributed, for numerical purposes, over a smooth profile described by the radial distribution S_i. For this article we used a Gaussian

$$S_i(\mathbf{x}-\mathbf{x}_i) = \frac{1}{\pi\sigma^2} \exp[-(\mathbf{x}-\mathbf{x}_i)^2/\sigma^2] \tag{5}$$

centered around a position $\mathbf{x}_i$ with a distribution width σ. The normalization constant in front of the exponential term, is chosen so that $\int S_i d\mathbf{x} = 1$, assuming an infinite large 2D space. It is easy to show by integrating Eq. (4) over an infinite large 2D space that this normalization gives eN_pZ_d as the total space charge contribution per unit length from all cylinders, as expected. Note that the charge on the particle is assumed azimuthally symmetric, without any dipole moment on the grain itself.

The distribution given in Eq. (5) is peaked at the center of the particle. This is unlike the hollow profile used in Ref. 2, where S_i was peaked at the nominal surface of the particle. Equation (5) allows easier numerical resolution for small particle sizes than in Ref. 2, but at the expense of realism as to where the charge resides on the particle. Here, the charge is distributed throughout the particle and is peaked in its center. The validity of this is limited to particles that are small compared to the shielding length, $a_d \ll \lambda_{De}$. Physically, an infinitesimal particle has a space charge distributed as a Dirac delta source $\delta_i(\mathbf{x}-\mathbf{x}_i)$ corresponding to a line in our 2D geometry. A line is theoretically equivalent to S_i, in the limit $\sigma \ll \lambda_D$. However, in the numerical solutions we must always work with a finite σ in order to resolve the diffuse object numerically. In problems where plasma shielding effects are of interest, the dimension of the computational domain L must be chosen significantly larger than λ_D (typically $L \sim 10-20\ \lambda_D$). Because of this, we normally have to use $\sigma \sim 0.5-0.25\lambda_D$ which gives a solution in the vicinity of S_i that is different from the one around δ_i. This difference becomes smaller in the far field (at a distance from S_i of the order of or larger than λ_D).

The charged particles in a dusty plasma interact through a Coulomb scattering, which is modeled in our simulation by the force acting on a diffuse particle due to the local electric field in the plasma. The literature contains reports of several theoretical studies of how diffuse objects collide compared with point objects in a thermal plasma.[13] Unfortunately, these studies are not applicable to our cold ion model. We are therefore limited only to do numerical tests where we, for instance, can change σ to see if this parameter has a profound influence on the solution. This is done in Sec. III.

Our 2D cylindrical particles differ in some ways from physical spheres in three dimension (3D). One important difference is in the capacity C of the objects. For a small sphere with radius $a_d \ll \lambda_D$, we can neglect shielding from the plasma, and use the capacity $C = 4\pi\epsilon_0 a_d$ of an isolated object. For a cylinder, however, we have to include the shielding due to the geometry. Since this shielding is rather complicated in a mesothermal plasma flow, we can only estimate this relation, for instance, from two concentric cylinders where the outer one is shielded at a distance λ_D. The capacity per unit length then becomes

$$C = 2\pi\epsilon_0 / \ln(1 + \lambda_D / a_d), \tag{6}$$

where the surface charge q_d per unit length of a cylinder is related to the surface potential U_0 by $q_d = CU_0$. It is important to notice that this capacity difference between 2D and 3D dust particles leads to two major differences between our simulation and a 3D simulation with spherical dust particles. First of all, we would have a different space charge contribution from spheres given by the parameter P and from a cylinder which is given by a redefined P value.[2,14] Second, the levitation of a cylinder will be different from a sphere due to a different q_d/m_d ratio.

C. Solution procedure

The orbits of the diffuse dust particles are followed by integrating their equations of motion. Interpolation is required since the positions of the diffuse particle centers $\mathbf{x}_i$ lie between the numerical grid points where the potential is calculated. For a δ_i distribution the plasma potential at $\mathbf{x}_i$ can be calculated from the interpolation or convolution integral $\phi(\mathbf{x}_i) = \int \phi(\mathbf{x})\,\delta_i(\mathbf{x} - \mathbf{x}_i)\,d\mathbf{x}$. This method can be adapted for the diffuse particles, which yields

$$\frac{d^2\mathbf{x}_i}{dt^2} = -\frac{eZ_d}{m_d}\int \nabla\phi(\mathbf{x}) S_i(\mathbf{x} - \mathbf{x}_i)\,d\mathbf{x} + \mathbf{g} - \eta\mathbf{u}_i\,. \tag{7}$$

Obviously, the use of S_i instead of δ_i introduces an error which becomes small when σ is small compared to the length scale of variation of $\nabla\phi(\mathbf{x})$ around location $\mathbf{x}_i$. Here we have also included gravity $\mathbf{g}$, which is important for large dust particles, and a friction force $-\eta\mathbf{u}_i$ for a dust particle with velocity $\mathbf{u}_i$. This friction force can be used to model collisions between dust particles and neutral particles, but it is also needed for numerical reasons. The dust kinetic energy often has to be reduced in the numerical solution before fluid and crystal-like structures can be seen.

The plasma potential $\phi(\mathbf{x})$ in Eq. (7) is calculated from Poisson's equation (4) which includes Boltzmann electrons, cold fluid ions, and the dust particles described by diffuse objects. Since the plasma fluid equations [Eqs. (1)–(4)] predict ion acoustic waves, we are able to model wave–particle interactions between this wave mode and the diffuse dust particles. A local ion acoustic wave is generated around each charged dust object due to electrostatic interaction and leads to an ion Coulomb drag force acting on the dust particles. This force will therefore appear in Eq. (7) through the potential $\phi(\mathbf{x})$. However, ion drag due to direct collisions between ions and dust particles is not included in our model, where we neglect ion absorption into the dust particles.

The time scale of the motion of dust particles is much slower than for electrons and ions. Thus, we can assume the plasma to always be in equilibrium when we compute the dust motion. In our calculations we relax the plasma until it reaches a stationary solution [$\partial_t \simeq 0$ in Eqs. (1) and (2)] for each time the dust particles are moved. These steps are then repeated until the dust particles settle into equilibrium positions where the forces acting on all dust particles are zero. Due to the friction force used in Eq. (7) and the absence of any energy input, the dust particles graduately damp into their equilibrium positions. The dust particle average kinetic energy,

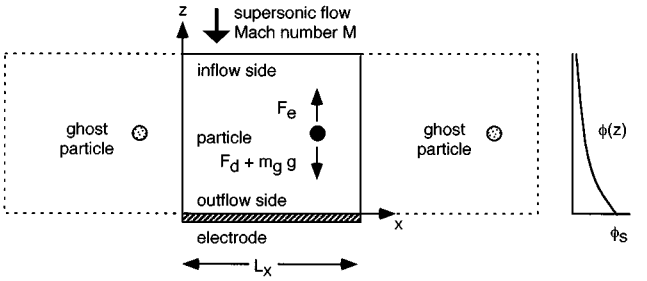

FIG. 1. Sketch of the simulation system showing a single dust particle confined in the sheath above a negatively biased electrode. Ions enter the sheath in the $-z$ direction with a specified Mach number $M > 1$. Our numerical approach assumes periodic and nonperiodic solutions in the x and z directions, respectively. Ghost particles due to periodic boundary conditions simulate a horizontal particle spacing of L_x.

$$E_k = \frac{1}{N_p}\sum_{i=1}^{N_p}\frac{1}{2}m_d|\mathbf{u}_i|^2, \tag{8}$$

will therefore approach zero as the dust particles obtain an equilibrium.

We also compute the average potential energy of the dust particles,

$$E_p = \frac{1}{N_p}\sum_{i=1}^{N_p}\{q_d[\phi(\mathbf{x}_i) - \phi_i(\mathbf{x}_i)] + m_d g z_i\}, \tag{9}$$

where $q_d\phi_i$ is the electrostatic energy contribution from the particle itself, which has to be subtracted from the total electrostatic energy $q_d\phi$.

III. RESULTS

In our numerical simulations we assume the ions to enter the 2D computation domain (x,z) in the counter z direction as shown in Fig. 1, with a supersonic velocity $-v_0$ or a Mach number $M = |v_0/c_i| > 1$ normalized to the ion acoustic velocity c_i. The solutions are assumed to be periodic in the x direction, and nonperiodic in the z direction so that boundary conditions can be imposed at $z = 0$ and $z = L_z$. On the inflow boundary $(z = L_z)$ we specify three conditions

$$\begin{aligned} v_{iz}(z = L_z) &= -v_0\,, \\ n_i(z = L_z) &= n_0\,, \\ \phi(z = L_z) &= 0 \end{aligned} \tag{10}$$

due to the supersonic inflow velocity. Here v_{iz} is the component of $\mathbf{v}_i$ in z direction (velocity component normal to the inflow boundary). The cold ions are then assumed to be accelerated towards a negatively biased electrode with respect to the potential on the inflow side (see Fig. 1). Since the flow is supersonic in the entire computational domain, ion acoustic waves are not able to propagate in the counterstream direction. This means physically that no ion acoustic wave

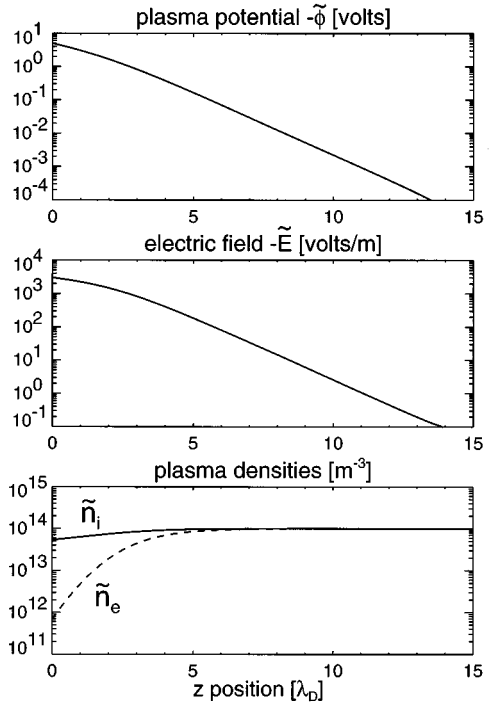

FIG. 2. Stationary plasma solution with no dust particles in the sheath. The parameters are $T_e=1$ eV, $n_0=10^{14}$ m^{-3}, $M=2$, and $\phi_s=-5$, corresponding to an electron Debye length of $\lambda_D=7.43\times10^{-4}$ m.

disturbance can propagate away from the electrode into the plasma, and that the plasma will feel only the electrostatic disturbance from the electrode. A consistent numerical treatment of this problem would therefore be to specify the potential

$$\phi(z=0)=\phi_s \tag{11}$$

on the outflow boundary, while values for n_i and v_{iz} at the electrode are computed from their differential equations.

To solve the set of equations for the plasma and the electrostatic field given by Eqs. (1)–(4) we have used a spectral method.[15] In this approach the solutions are expanded in terms of Chebyshev and Fourier polynomials in the z and x directions, respectively.[2,15]

A solution for a dust-free sheath was found as a stationary solution of Eqs. (1)–(4). This solution, shown in Fig. 2, is the same as for the well known cold ion model for sheaths.[16] In Fig. 2 we have used the parameters $M=2$, $T_e=1$ eV, and $n_0=10^{14}$ m^{-3} to model the conditions of a low-density gas discharge. The corresponding electron Debye length is $\lambda_D\simeq7.43\times10^{-4}$ m, which is used to normalize the units of the z axis in Fig. 2. The electrode is biased to $\phi_s=-5$ V.

The sheath is perturbed by the presence of charged dust particles. In Figs. 3(a) and 3(b) we show the perturbations in the density and plasma potential caused by a pair of stationary particles aligned side by side with respect to the flow direction. These are shown as the solutions with particles minus the solutions without particles as shown in Fig. 2. Note the ion focus regions downstream of the particles where the ion density is enhanced and the plasma potential is more positive. There is an anisotropic potential around a particle, and the positive charge of the ion focus region can attract a negatively charged particle.

The calculations in Fig. 3 were repeated for two different values of the diffuse particle width $\sigma=0.5\ \lambda_D$ and $0.25\ \lambda_D$ to see how this numerical parameter affects the results. The particles are centered at $(x,z)=(2.5,11.25)$ and $(7.5,11.25)$. In Fig. 3(a) notice the much stronger ion focus-

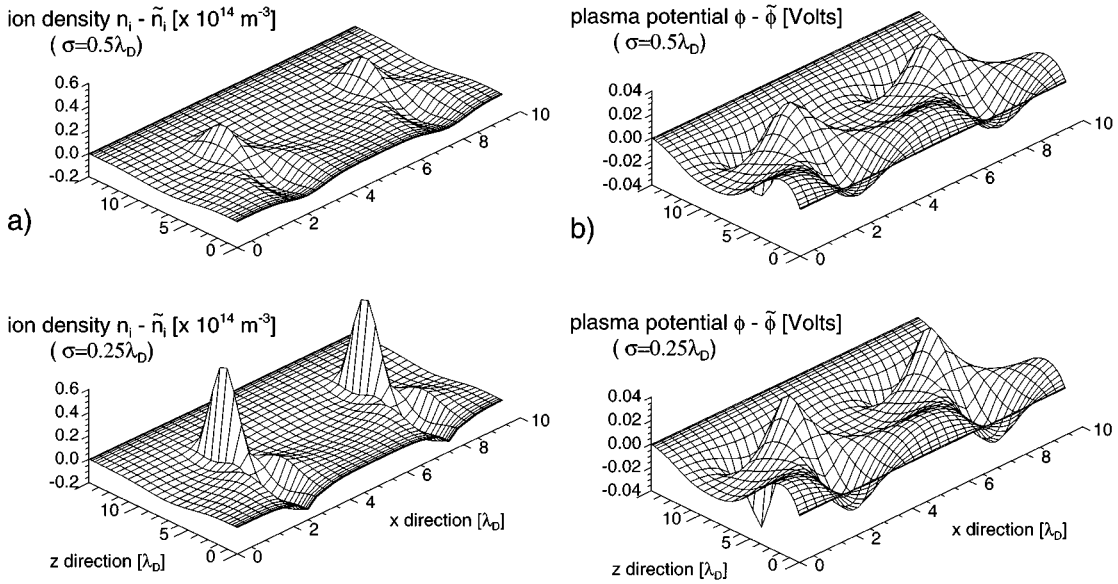

FIG. 3. Perturbation in the ion density (a) and plasma potential (b) due to two negatively charged cylinders aligned side by side with respect to the ion streaming direction. Both cylinders have a surface potential $U_0=-0.5$ V and a surface radius $a_d=0.1$ μm used in the capacity [Eq. (6)] to find the dust charge per unit length. We show solutions for two different widths ($\sigma=0.5\ \lambda_D$ and $0.25\ \lambda_D$) of the diffuse cylinder [Eq. (5)]. The other parameters are the same as for Fig. 2.

ing on the downstream side of the particle locations for $\sigma = 0.25\ \lambda_D$ than for $0.5\ \lambda_D$. This difference in ion density becomes smaller as we move closer to the electrode and enter an area of reduced ion density. The plasma potential, Fig. 3(b), however, shows very little difference between the upper and lower figures, except close to the particle locations. This indicates that this potential distribution is close to the one for two lines (δ_i distributions) in the far field. We would therefore expect that these diffuse objects will model collisions between small cylindrical dust particles ($a_d \ll \lambda_D$) very accurately, as long as the particles do not come too close as they collide. The ion flux cannot, however, be modeled accurately in the vicinity of the charged objects or in the ion focusing region due to the large difference in ion density between the lower and upper panels in Fig. 3(a).

The strong ion focusing that occurs on the downstream side of a negatively charged object [Fig. 3(a)] will lead to a region where the plasma potential goes positive [Fig. 3(b)]. This region has previously been suggested to be responsible for the vertical alignment of dust particles in dust crystal structures[2] and trapping of other negatively charged dust particles.[1] We shall now use our simulation to assess how important this ion focusing effect is for the formation of dust crystals.

By using a simple system of only two particles under the influence of gravity in the sheath, we searched for equilibria and found results that are very illuminating for understanding the interparticle potential. The equilibrium is bistable. Depending on the particles' initial positions, they settle either into a side-by-side equilibrium or a vertical column. When they were initially side by side, they stayed that way. The final separation between the particles in the x direction was $L_x/2$ where L_x is the size of the computation domain in the x direction. This separation can be understood in view of the periodic boundary conditions used in this direction which introduce ghost dust particles outside the computational domain. These ghost particles confine the dust in the x direction and create a minimum in the potential energy [Eq. (9)] at particle separation $L_x/2$. In the other direction (z direction), the final levitation height of the dust particles above the electrode will be determined by the force balance between gravity and the electrostatic force. The latter includes both an electrostatic force caused by the sheath F_e and the ion Coulomb drag force F_d, as illustrated in Fig. 1.

However, when we aligned the two particles initially on top of each other, that is how they remained. The downstream particle settled close to the potential maximum generated by the upstream particle.

Further runs with two particles distributed randomly in space show that only these two final orientations (aligned side by side and on top of each other) are possible. To determine which of these alignments is most likely, one can compare the average potential energy, defined by Eq. (9), for the configurations. Denoting these as E_{p1} and E_{p2} for side-by-side and vertical (on top of each other) alignments, respectively, we found that $E_{p2}/E_{p1} > 1$ when L_x is so large that the potential interaction from the ghost particles outside the computational domain can be neglected. For these conditions the horizontal alignment is most likely, since it has the lowest potential energy. As L_x is made smaller, we eventually reach a point where $E_{p2}/E_{p1} < 1$, and vertical alignment becomes most likely. This is due to the electrostatic interaction from the ghost particles.

Numerical results also show that the dust charge-to-mass ratio q_d/m_d has a profound influence on E_{p2}/E_{p1}. By reducing q_d we reduce the ion focusing and therefore the potential maximum generated by the upstream particle. As a result, we obtain a smaller E_{p2}/E_{p1} ratio. We also see a reduction in this ratio when m_d is increased. This is due to a larger gravitational influence, which makes the side-by-side alignment preferable.

As we increase the number of dust particles, we get a larger number of possible crystal structures. A system containing $N_p = 6$ particles can theoretically settle to one of 13 different crystal configurations. We carried out numerical simulations with six particles to find their final equilibria, where we initially distributed the particles randomly in space with zero velocity. We did not detect all 13 possible arrangements. Those we did not detect are either unstable or stable, with a small probability of being realized. Of course some of these might be seen with other parameters for the simulation domain, etc. than we assumed in our runs. For example, a configuration with six particles on top of each other is one that we never saw. Very likely it is not stable to transverse displacements, due to gravity. Then again, perhaps it would be a possible configuration if the size of our computational domain in the z direction were smaller.

In Fig. 4 we show how six particles come to equilibria. Three different sets of random initial positions were used, and these led to two different equilibrium configurations. They are the vertically aligned and staggered arrangements that have been observed in experiments.[3,7–9] This result verifies that the vertically aligned structures are due to the anisotropic effect of ion focusing in a flowing plasma. It also agrees with the experiments in demonstrating that the vertical alignment is not the only stable equilibrium. A staggered arrangement as in a bcc crystal is also possible. The plasma and dust parameters for Fig. 4 are given in the Fig. 4 caption.

The time evolution of the average kinetic and potential energy, defined in Eqs. (8) and (9), respectively, are shown in Fig. 5. Here we see, as expected, that the potential energy for each run approaches a constant value as the gas drag cools the particles and their kinetic energy approaches zero. We also see that the final potential energy of the vertically aligned particles in runs 1 and 3 is identical as expected, and that the staggered particle arrangement in run 2 has a higher final potential. The final configuration with three particles in a vertical column (see Fig. 4) is, therefore, the most probable for the parameters we used. However, by changing q_d/m_d or L_x, we got other crystal alignments, where sometimes a crystal with columns of differing numbers had the smallest potential energy.

Interesting particle arrangements are found when the number of particles in the simulation box is increased. In

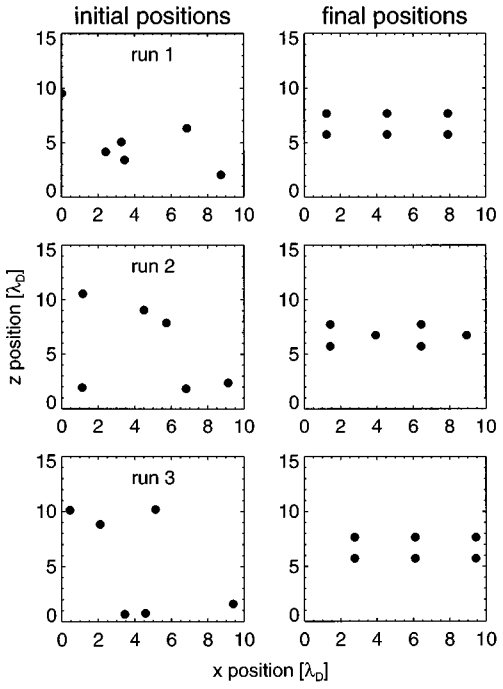

FIG. 4. Initial and final positions obtained from the simulation for $N_p=6$ dust particles. The particles are initially distributed in three different random positions (runs 1–3) with zero velocity. The parameters are $T_e=1$ eV, $n_0=10^{14}$ m^{-3}, $M=2$, $\phi_s=-5$ V, $U_0=-1$ V, and $a_d=0.1$ μm, and a dust material density $\rho_d=10^3$ kg/m^3.

Fig. 6 we have increased the number of particles to $N_p=48$ and reduced the q_d/m_d ratio. The equilibrium has an arrangement with particles in multiple layers. Comparing the top and bottom layers, there are more particles in the lowest layer (14) than in the uppermost (7). In effect, the horizontal lattice constant is not the same for the top and bottom layers. Due to this, it is impossible for the crystal to form either simple columns or staggered layers with equal spacing, as we have already observed in the simulation with a smaller number of particles. Instead, the crystal has a more complicated arrangement.

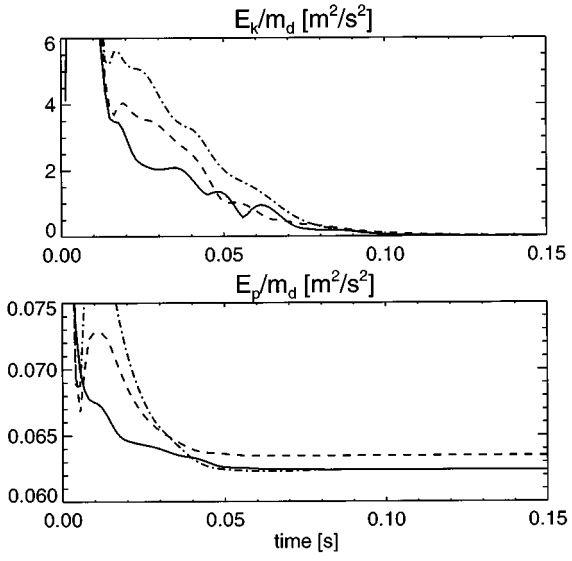

FIG. 5. Time evolution for the average dust particle energy-to-mass ratios E_k/m_d and E_p/m_d for the solutions shown in Fig. 4. Here E_k is the dust average kinetic energy [Eq. (8)] while E_p is the average potential energy [Eq. (9)].

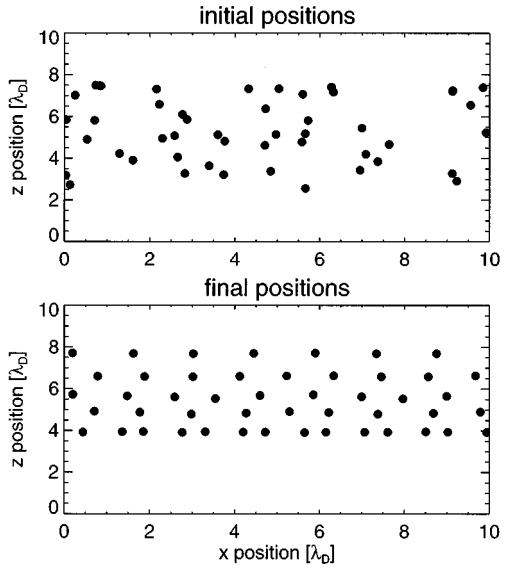

FIG. 6. Initial and final positions for a system containing $N_p=48$ diffuse dust particles. The other parameters are $T_e=1$ eV, $n_0=10^{14}$ m^{-3}, $M=2$, $\phi_s=-5$ V, $U_0=-0.5$ V, $a_d=0.15$ μm, and $\rho_d=10^3$ kg/m^3.

IV. DISCUSSION

Our numerical results show that dust particles confined by an electrostatic field and gravity have equilibria in both side-by-side and vertically aligned arrangements. The latter alignment is caused by the ion focusing downstream of a negatively charged particle. This leads to an attractive force that pulls one negatively charged particle directly below another so that it rests in the local maximum in the plasma potential, as shown in Fig. 3. This kind of trapping may happen randomly and leads to a number of different equilibria where the force acting on each dust particle is zero. Different sets of initial conditions might therefore give different alignments, as shown in Fig. 4. Each alignment has a discrete potential energy E_p (Fig. 5) where the alignment with the lowest potential has the greatest probability for occurring. The potential energy E_p for each alignment is strongly correlated to the q_d/m_d ratio and to the L_x dimension of the computation domain. In a physical dusty crystal it would probably be possible to get transitions between different equilibrium alignments due to, for instance, thermal motions of dust and low frequency fluctuation in the electric field.

Dust plasma crystals that are observed in experiments often show regular 3D structures that can be identified as hexagons, bcc, and fcc crystals.[3–9] A 3D crystal can, of course, not be obtained in our 2D simulation, but we would expect to

get regular 2D structures if we ran our simulation under the same conditions as in these experiments. There are, however, a number of numerical limitations that make this difficult. As an example, our 2D objects have a different capacity than a sphere and a corresponding different space charge contribution from the objects and different q_d/m_d ratios. We would, for instance, get a factor of ~ 3 larger q_d/m_d ratio if we had used spheres instead of cylinders with the same surface potential, material density, and radius. The focusing of ions around the object would also have been larger around a sphere than a cylinder due to the geometry.[2] This enhanced focusing suggests that, together with the larger q_d/m_d ratio, the ion stream effect probably is important for much larger spherical dust particles than for the small size $a_d \simeq 0.1$ μm cylinders we used.

The periodic boundary condition in the x direction may also impose nonphysical interactions between the simulated dust particles and the ghost particles outside the computational domain. We need, for instance, a large number of numerical dust particles to get the motion of a dust particle not correlated with the motion of the corresponding ghost particle. Other simplifications which may be inaccurate are the constant dust charge and the neglect of ion–neutral collisions. Previous studies of dust charge variation in, for example, Ref. 17, show that the dust charge may vary considerably over the sheath due to variations in n_e and n_i. Local effects, such as ion focusing around objects, may also change the ion flux into one particle as it enters the wake of another.[2,18] Ion neutral collisions will change the structure of this wake when the ion–neutral collision mean free path approaches the dimension of the wake. This might be an important effect in gas discharges with relatively large neutral pressure. A general and accurate numerical simulation of dust particle crystallization must therefore be done in 3D with nonperiodic boundary conditions in all directions, including an accurate model for charge variation and ion–neutral collisions.

It is possible to use the analytical approximation given in Ref. 1 to estimate the conditions where the attractive force between charged dust particles becomes important compared to, for instance, gravity. In Ref. 1 the authors obtain the plasma potential

$$\phi(z) = \frac{eZ_d}{2\pi\epsilon_0|z|}\cos\left(\frac{|z|}{L_s}\right) \tag{12}$$

on an axis going through an isolated negatively charged sphere parallel to the ion flow direction. Here z is the distance from the particle on the downstream side while L_s is a length scale determined by the Debye length and the Mach flow number $L_s = \lambda_D (M^2 - 1)^{1/2}$. Potential (12) assumes that $M > 1$, a large distance from the charged object and long wavelengths compared to λ_D. This potential has a maximum and a minimum close to $z = \pi L_s$ and $2\pi L_s$, respectively. We find the ratio ϵ between the electrostatic energy corresponding to this potential difference and the gravitational energy required to remove a negatively charged dust particle from the potential well to be

$$\epsilon \simeq \frac{n_0 K T_e}{a_d \rho_d g (M^2 - 1)}\left(\frac{eU}{KT_e}\right)^2. \tag{13}$$

For plasma parameters that can apply to gas discharges ($n_0 = 10^{15}$ m^{-3}, $T_e = 1$ eV) and dust particles with size $a_d = 1-10$ μm which is typical for dust in plasma crystal experiments,[5–9] we obtain $\epsilon \sim 10^{-1} - 10^{-2}$. We have assumed here a dust material density of $\rho_d = 10^3$ kg/m^{-3} and a dust surface potential of $eU/KT_e = 4$. For such small values of ϵ, gravity should be able to remove a charged dust particle from the attractive potential well. However, other forces such as the ion drag force, thermophoretic force, and the electrostatic force from the sheath will nearly cancel out gravity in the regions where the dust particles are trapped and make the net force acting on a dust particle considerably less than gravity. Equation (13) therefore underestimates the importance of the attractive force. Another problem with this estimate is that some of the dust and plasma parameters used in Eq. (13) are rather uncertain. This is especially the case for the dust surface potential eU/KT_e in rf discharges. Here eU/KT_e probably varies a lot between individual experiments since it is strongly correlated to the rf amplitude on the electrodes and the position of dust particles in the sheath.

Even though Eq. (13) and the numerical approach we used both include a number of physical simplifications, they are probably able to give a good illustration of the importance of anisotropic effects due to ions flowing toward the electrodes. In the numerical solutions we obtain both a random crystal structure in Fig. 4 and a more regular dust crystal in Fig. 6 as we increase N_p and decrease the q_d/m_d ratio used in Fig. 4. The reason for this regularity is the reduced q_d/m_d ratio where the particle trapping effect no longer has a profound influence on the crystal structure. Long vertical alignments which may occur due to the random particle trapping have zero or very small probability. This particle alignment is therefore strongly influenced by gravity which gives a constant vertical extension of the crystal.

ACKNOWLEDGMENTS

The authors thank Dan Dubin and Tore Nitter for helpful discussions. Work by one of the authors (F. M.) was supported by The Research Council of Norway, and the second author (J. G.) was supported by NASA and the National Science Foundation.

[1] M. Nambu, S.V. Vladimirov, and P.K. Shukla, Phys. Lett. A **203**, 40 (1995).
[2] F. Melandsø and J. Goree, Phys. Rev. E **52**, 5312 (1995).
[3] J.H. Chu and I. Lin, Phys. Rev. Lett. **72**, 4009 (1994).
[4] G. Praburam and J. Goree, Astrophys. J. **441**, 830 (1995).
[5] Y. Hayashi and K. Tachibana, Jpn. J. Appl. Phys. **33**, L804 (1994).
[6] H. Thomas, G.E. Morfill, V. Demmel, J. Goree, B. Feuerbacher, and D. Möhlmann, Phys. Rev. Lett **72**, 4009 (1994).
[7] J. B. Pieper, J. Goree, and R.A. Quinn, J. Vac. Sci. Technol. A **14**, 519 (1996).
[8] G.E. Morfill and H. Thomas, J. Vac. Sci. Technol. A **14**, 490 (1996).
[9] Y. Hayashi and K. Tachibana, J. Vac. Sci. Technol. A **14**, 506 (1996).
[10] R.T. Farouki and S. Hamaguchi, Appl. Phys. Lett. **61**, 2973 (1992).
[11] Ya. L. Al'pert, L. Gurevich, A. Quarteroni, and L.P. Pitaevskii, *Space Physics with Artificial Satellites* (Consultants Bureau, New York, 1965).
[12] E. Coggiola and A. Soubeyran, J. Geophys. Res. A **5**, 7613 (1991).

[13]H. Okuda and C.K. Birdsall, Phys. Fluids **13**, 2123 (1970).
[14]O. Havnes, T.K. Aslaksen, and F. Melandsø, J. Geophys. Res. **95**, 6581 (1990).
[15]C. Canuto, M.Y. Hussaini, A. Quarteroni, and T.A. Zang, *Spectral Methods in Fluid Dynamics* (Springer, New York, 1988).
[16]F.F. Chen, in *Plasma Diagnostic Techniques*, edited by R.H. Huddlestone and S.L. Leonard (Academic, New York, 1965).
[17]T. Nitter, T.K. Aslaksen, F. Melandsø, and O. Havnes, IEEE Trans. Plasma Sci. **22**, 159 (1994).
[18]S.J. Choi and M.J. Kushner, J. Appl. Phys. **75**, 3351 (1994).